Photovoltaic properties of conjugated polymer/methanofullerene composites embedded in a polystyrene matrix

Brabec, C. J.; Padinger, F.; Sariciftci, N. S.; Hummelen, J. C.

Published in:
Journal of Applied Physics

DOI:
10.1063/1.370205

Publication date:
1999

Photovoltaic properties of conjugated polymer/methanofullerene composites embedded in a polystyrene matrix

C. J. Brabec,[a] F. Padinger, and N. S. Sariciftci
Christian Doppler Laboratory for Plastic Solar Cells, Johannes Kepler University Linz, A-4040 Linz, Austria

J. C. Hummelen
Stratingh Institute and Materials Science Center, University of Groningen, Nijenborgh 4, 9747 AG Groningen, The Netherlands

(Received 13 October 1998; accepted for publication 3 February 1999)

Bulk donor–acceptor heterojunctions between conjugated polymers and fullerene derivatives have been utilized successfully for photovoltaic devices showing monochromatic energy conversion efficiencies above 1%. The photovoltaic response of these devices is based on the ultrafast, photoinduced electron transfer from the conjugated polymer to the fullerene [N. S. Sariciftci and A. J. Heeger, *Handbook of Organic Conductive Molecules and Polymers*, (Wiley, New York, 1997), pp. 413–455]. In this work we present efficiency data of solar cells based on a soluble derivative of *p*-phenylene vinylene (PPV), poly [2-methoxy, 5-(3′,7′-dimethyl-octyloxy)]-*p*-phenylene vinylene (MDMO-PPV), and a highly soluble methanofullerene, [6,6]-phenyl C_{61}-butyric acid methyl ester (PCBM), embedded into a conventional polymer, polystyrene (PS). By the blending of the optimized donor–acceptor components into the conventional polymer matrix, the percolation threshold for photovoltaic response of the three component systems is found to be determined by percolation of the methanofullerene in the polymer matrix. We present current/voltage data of PS–MDMO-PPV–PCBM devices with various PS concentrations as well as photoinduced absorption studies in the infrared [(PIA) Fourier transform infrared] and light induced electron spin resonance studies on the electron transfer in these composites. At low light intensities, the monochromatic power conversion efficiency η_e and the photon carrier collection efficiency η_c of the PS free device are calculated with 1.5% and 18%, respectively. © *1999 American Institute of Physics.* [S0021-8979(99)08609-0]

I. INTRODUCTION

The ability to dope conjugated polymers over the full range from insulating to conducting behavior resulted in emphasized research in this class of materials that combines the electronic and optical properties of semiconductors and metals with the attractive mechanical properties as well as processing properties of polymers.[1–4] A wide class of these conjugated polymers and oligomers shows a subpicosecond photoinduced electron transfer from the excited state of the conjugated polymer onto C_{60},[5–7] which is a good electron acceptor capable of accepting as many as six electrons.[8] The electron transfer to C_{60} quenches both the strong photoluminescence and the intersystem crossing[9] of the polymer.

Energy conversion efficiencies of various organic solar cells, including small molecular[10,11] as well as polymeric solar cells[12,13] are typically in the range of 1%. However, because of the inherent processing advantages that are offered by polymer-based solar cells, like large scale roll-to-roll production on flexible substrates, those devices are potentially more attractive for commercialization. Presently, the highest efficiencies were achieved with fullerenes[14] or conjugated polymers[15] as acceptors.

Spectroscopic studies showed that the photoinduced electron transfer between conjugated polymers and fullerenes occurs on a time scale smaller than 200 fs.[5] Since this is faster than any other known relaxation mechanism in the conjugated polymer, the quantum efficiency of this process is estimated to be close to unity. However, the power conversion efficiency of conjugated polymer/fullerene photovoltaic devices is limited by inefficient collection of the charges at the electrodes[16] due to the low mobility of the holes on the conjugated polymer and the electrons on the fullerenes. The low mobility of the carriers is a consequence of the hopping conduction in the network. Conduction by thermally assisted hopping transitions between spatially separate sites in an interpenetrating network[17] can be modeled by percolation theory. Following percolation theory the formation of interconnected paths of small spherical molecules embedded in a three dimensional matrix occurs at a volume fraction of 17%.[18] This was experimentally verified by photocurrent measurements in conjugated polymer–fullerene devices.[19] Additionally, it was found that higher concentrations of the fullerene (methanofullerene, but also pristine C_{60}) relative to the conjugated polymer (typically 3:1) increase the power efficiency by increasing the short circuit currents.[14,16] This is again in accordance with percolation theory, where the average conductivity σ of one component may be expressed by the following equation:

[a]Electronic mail: christoph.brabec@jk.uni-linz.ac.at

$$\sigma = \frac{1}{l} Z_c^{-1}. \quad (1)$$

Here 1 is a characteristic length depending on the concentrations of the sites, while Z_c is the resistance of the path with the lowest average resistance. According to Eq. (1), high fullerene concentrations enhance the conductivity by two mechanisms. First, the higher concentration of sites decreases 1, and second, new paths with a lower overall resistance Z_c may be formed. At high mixing ratios of 3:1, excellent solubility of the fullerene, as well as good compatibility between the conjugated polymer and the fullerene is necessary.

The embedding of the photoactive conjugated polymer–fullerene blend in a polystyrene matrix (guest–host approach) presented in this article is a sound and promising method to improve the photoactive sample quality for the following reasons:

(1) The conjugated polymer diluted by the polystyrene host matrix shows less interchain interaction compared to pure films.
(2) Macroscopic ordering of the conjugated polymer can be performed by mechanical stretching of the host polymer.
(3) The stability of the conjugated polymer–fullerene devices under ambient conditions (i.e., in the presence of water or oxygen) limits the practical application. Recent Fourier transform infrared (FTIR) degradation studies on the polymer composites showed rapid bleaching of the conjugated polymer and somewhat slower degradation of C_{60} under oxygen and light.[20] Stabilization of these composites was realized by the exclusion of oxygen, either by sealing or by handling the devices under inert conditions. In the guest–host approach the conjugated polymers are better encapsulated against environmental influences.
(4) By the choice of a proper host matrix the charge transfer between conjugated polymer and fullerene may be advantageously tuned, either by changing the intermolecular distances due to morphology control or by the overall dielectric constant of the system.

This study is focused on a soluble alkoxy-*p*-phenylene vinylene (PPV) poly [2-methoxy, 5-(3′7′-dimethyl-octyloxy)]-*p*-phenylene vinylene (MDMO-PPV) as photoactive polymer; earlier studies on similar alkoxy-PPVs (MEH-PPV-poly [2-methoxy, 5-(2′-ethyl-hexyloxy)]-*p*-phenylene vinylene) have been reported.[21,22] Alkoxy-PPVs are known for their high incident photon to carrier conversion efficiency (IPCE) with an electron acceptor like [6,6]-phenyl C_{61}-butyric acid methyl ester (PCBM).[14] Furthermore, the high solubility of these materials allows homogenous, thin film formation from solutions with optical quality. Another essential point is the partial chemical similarity and the subsequent compatibility of the alkoxy-PPVs and the substituted methanofullerenes. This favors the formation of homogenous blends and prevents aggregation or separation of the two components, thereby avoiding the formation of short circuits between the electrodes of the devices. Devices with different concentrations of polystyrene (PS) were fabricated and characterized by current–voltage ($I-V$) measurements under monochromatic light and by wavelength dependent photocurrent measurements. From these data power efficiencies were calculated and compared to the electron–photon conversion efficiencies.

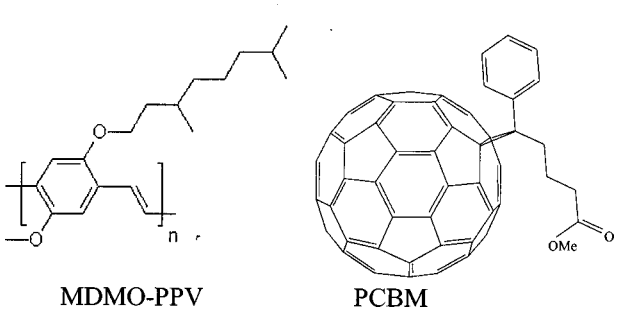

MDMO-PPV PCBM

FIG. 1. Chemical structure of MDMO-PPV and PCBM.

II. EXPERIMENT

Photovoltaic devices were produced by spin casting from 1,2-dichlorobenzene (ODCB) solution under room temperature conditions. For the solar cells MDMO-PPV was used as the electron donor, while the electron acceptor was PCBM.[23] The chemical structure of the compounds is shown in Fig. 1. The enhanced solubility of PCBM compared to C_{60} allows a high fullerene–conjugated polymer ratio and strongly supports the formation of donor–acceptor bulk heterojunctions. High optical quality films with high weight ratios of PCBM: alkoxy PPV are possible.[16] For the PS blends we have used a Hostyren PS N 168 (Hoechst AG). Solutions for spincasting were prepared with such concentrations, that the percentage of the MDMO-PPV is approximately 0.2–0.5 wt%, depending on the concentration of the PS and PCBM. The weight concentrations of the PS in the devices were 0%, 11%, 20%, 33%, 50%, 66%, and 80%, while the weight ratio of the fullerene on the conjugated polymer was kept at 3:1 for all cells.

Cleaned indium–tin–oxide (ITO) substrates have been used as transparent conducting electrodes.[24] The typical film thickness of the spincast films was around 80–150 nm as determined from the optical density measured with a Hitachi absorption spectrometer. After a drying step the nontransparent aluminum top electrode was evaporated. Samples were mounted in a liquid nitrogen bath cryostat with the electrical contacts formed by mechanical pressed spring leaves. The vacuum during the measurement was better than 10^{-5} Torr. The samples were illuminated on the ITO side through the quartz window of the cryostat by either a defocused Ar^+ laser beam at 488 nm or for the spectrally resolved measurements by a Xe arc lamp with a Czerny–Turner single pass monochromator. The illumination intensity was kept constant at 1 mW/cm^2 at each wavelength in the range between 400 and 700 nm. For consistency the $I-V$ characteristics of a PS free photodiode was recorded with the different illumination sources at equal light intensitities. Comparable values were found for both light sources, i.e., for the monochromatic xenon arc lamp light at 488 nm and 1 mW/cm^2 and for

the defocused Ar^+ laser at 488 nm and 1 mW/cm^2. Light intensities were measured by a calibrated Si photodiode. $I-V$ curves were recorded by a Keithley 2400 source meter, typically by averaging 200 measurements for one point. Photoinduced FTIR (PIA-FTIR) and light induced electron spin resonance (LESR) measurements were performed on a composite with equal weight ratios of PS–MEH-PPV–PCBM (1:1:1). Also C_{60} was used instead of PCBM in some experiments. These samples were prepared from approximately 1 wt% solutions in xylene. Infrared spectra were recorded on a Bruker IFS 66S spectrometer with a liquid nitrogen cooled mercury–cadmium–telluride (MCT) detector. The samples for these experiments were prepared by drop casting from polymer solution on KBr pellets. After evaporation of the solvent in a nitrogen laminar flow box, the pellets were mounted on the cold finger of a liquid nitrogen bath cryostat with ZnSe windows. The vacuum during all measurements was better than 10^{-5} Torr. The infrared absorption spectra of the photoinduced charges on the conjugated polymer were measured by accumulating ten single beam spectra under illumination of the polymer sample and referencing them to ten accumulated single beam spectra taken in the dark. The samples were illuminated through a quartz window of the cryostat by an Ar^+ laser (488 nm, 20 mW/cm^2). For a better signal-to-noise ratio 200 repetitions of the measuring sequence described above were accumulated.

LESR measurements were performed on a Bruker EMX spectrometer with a 200 MHz broadband bridge and a rectangular high Q cavity. The samples were illuminated by an Ar^+ laser (488 nm, 70 mW) through a 50% grid in the front of the cavity. Samples for LESR investigations were prepared in 3 mm Wilmad electron paramagnetic resonance (EPR) tubes from solutions with concentrations as described above. After pouring approximately 0.2 ml of polymer solution into the ESR tube the solvent was evaporated. After complete drying the inner side of the tubes was covered with the composite film. The tubes are evacuated down to 10^{-5} Torr and sealed.

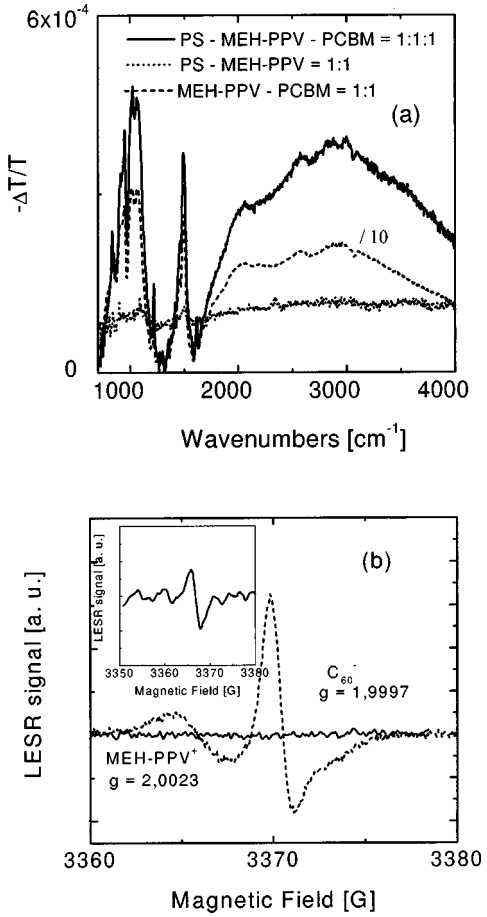

FIG. 2. (a) PIA FTIR spectra of three different compounds: PS–MEH-PPV–PCBM=(1:1:1), solid line (—); PS–MEH-PPV=(1:1), dotted line (·····), and MEH-PPV–PCBM (1:1), divided by a factor 10 and plotted by a dashed line (---). (b) LESR-spectra of MEH-PPV [solid line (—)] and PS–MEH-PPV–C60 (1:1:1) [dashed line (– – –)]. For LESR studies C_{60} was chosen instead of PCBM, as PCBM has a separate LESR signal in the investigated region. The inset shows a LESR spectrum of PS with 14 wt % of MEH-PPV and C_{60}.

III. RESULTS AND DISCUSSION

As shown by the PIA-FTIR studies displayed in Fig. 2(a), at equal concentrations of the three components (PS/MEH-PPV/PCBM=1:1:1) the photoinduced electron transfer is clearly observed. Both, the photoinduced infrared activated vibrational bands[25–27] (IRAV bands) observed in the range between 700 and 1700 cm^{-1} and the in-the-gap absorption around 3000 cm^{-1} due to the photoinduced polarons evidence the transfer of electrons from the polymer to PCBM. Furthermore, LESR measurements [Fig. 2(b)] show the two characteristic microwave absorption peaks of a photoinduced charge transfer between a conjugated polymer and a fullerene: one peak with a g value around 2.0023 (polaron$^+$ on the polymer) and one peak with a g value $<2(C_{60}^-)$. The inset in Fig. 2(b) shows the LESR spectrum of a composite with 14 wt % MEH-PPV and 14 wt % C_{60} in PS. No fullerene anion LESR signal was detected at high fields ($g<2$). In these samples the photoinduced charge separation was either very weak or even absent. This result is surprising, because the strong luminescence quenching in these samples indicated a nonradiative relaxation path of the photoexcitation. Since the observation of a steady state LESR signal requires a long living charge separated state, it is safe to conclude that for dilute concentrations of the photoactive components in the PS matrix, either the photophysics of the electron transfer is hindered by large distances of the donor and acceptor couple and/or the long living charge separated state is not longer achieved.

The absorption spectrum of the photovoltaic devices, shown in Fig. 3, is a linear superposition of the absorption spectrum of MDMO-PPV and PCBM (inset in Fig. 3). The influence of the PS matrix is indirectly noticed by the decreasing total optical thickness of the devices. At very high PS concentrations (66% and 80%) the spectrum is determined by the scattering background due to the PS with no detectable color in the visible. The formation of charge transfer complexes, recently reported for polyvinylcarbazole–fullerene blends,[28] was not observed between any of the components with PS.

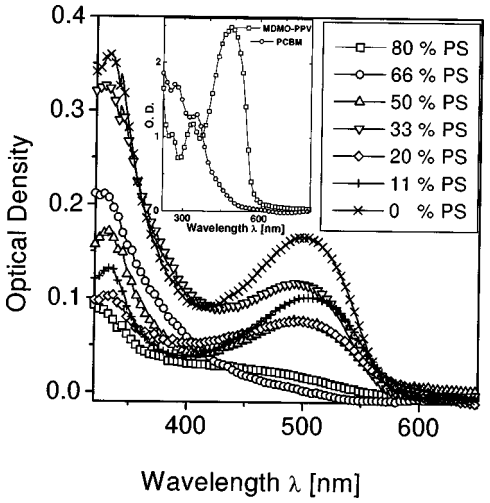

FIG. 3. Optical density of various PS–MDMO-PPV–PCBM devices. The optical density does not increase steadily with decreasing PS amount, as cells have been produced from different solutions. The inset shows the absorption spectra of the separate components [MDMO-PPV (□) and PCBM (○)]. The peak at 490 nm is attributed to MDMO-PPV absorption, while PCBM shows a first absorption maximum around 370 nm.

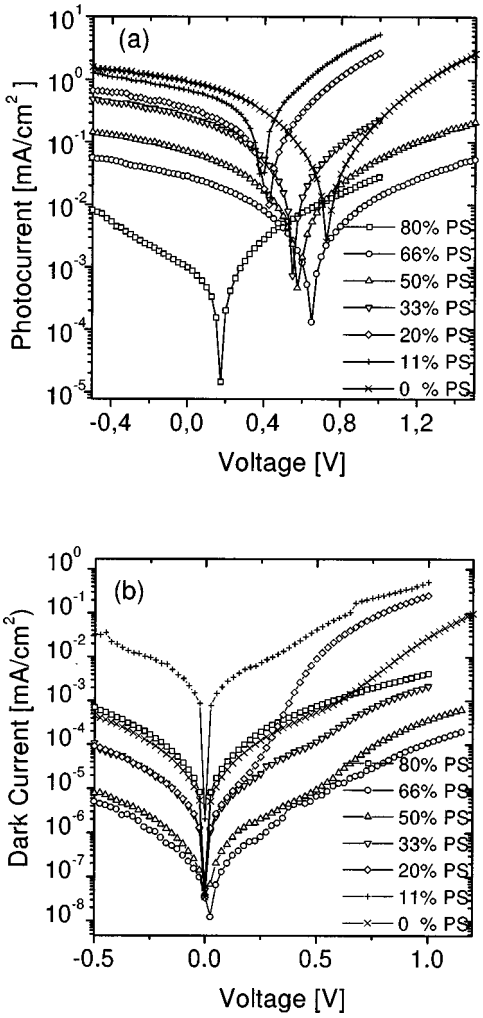

FIG. 4. (a) Short circuit current I_{sc} of various PS–MDMO-PPV–PCBM devices vs applied voltage with the concentrations denoted. Samples were measured under a vacuum better than 10^{-5} mbar when illuminated by 10 mW/cm^2 at 488 nm by a defocused Ar laser beam. (b) Dark current vs applied voltage for the PS–MDMO-PPV–PCBM devices with the concentrations denoted.

The PS concentration of the devices was varied between 0 and 80 wt % while the weight ratio of PCBM:MDMO-PPV was kept at 3:1. The $I-V$ characteristics of an ITO/MDMO-PPV–PCBM/Al photovoltaic device is compared with ITO/PS–MDMO-PPV–PCBM/Al devices in Fig. 4(a). The cells were illuminated through the ITO side with 10 mW/cm^2 at 488 nm. The dark current measurements are plotted in Fig. 4(b). At zero bias the PS free device showed a short circuit current I_{sc} of up to 0.85 mA/cm^2 and an open circuit voltage V_{oc} of 720 mV. Addition of PS did not alter the shape of the $I-V$ curves but affected the absolute values. The short circuit currents I_{sc} as well as the dark currents decreased with the addition of PS. The decrease of the dark current upon the increase of PS is ascribed to an ohmic contribution of PS to the total device resistance.

The observation of an unexpectedly high V_{oc} of 720 mV for the PS free device cannot be explained. The open circuit voltage for metal–insulator–metal (MIM) diodes is generally accepted to arise from the work function difference of the two electrodes[29] which would yield a V_{oc} of 0.4 V (Al 4.3 eV; ITO 4.7 eV) or lower for our devices.[30,31] Consistent with the MIM diode picture, the V_{oc} for single layer MEH-PPV devices sandwiched between ITO and Ca was found to follow the difference in the electrode work functions.[32,33] Using an Al electrode instead of Ca, the V_{oc} decreased slightly compared to devices with a Ca electrode but remained much higher than the difference of the work functions of Al and ITO.[32,33] In donor–acceptor bilayer photocells V_{oc} has a different physical origin. Studies on bilayer devices of ITO/MEH-PPV–C_{60}/Au showed[34] that the MEH-PPV–C_{60} interface yields under intense illumination an open circuit voltage around 0.53 V. This value of V_{oc} seems to be indicative for the MEH-PPV–C_{60} interface with nonrectifying metal contacts.

In two component charge transfer systems such as in the bulk-heterojunction solar cells presented here, deviations of V_{oc} from the results of pristine single layer or bilayer devices are expected for two reasons: First, some part of the available difference in electrochemical energy is consumed internally by the charge transfer to a lower energetic position on the electron acceptor. Second, the relative position of the lowest unoccupied molecular orbital (LUMO) of the electron acceptor may be below the work function of the cathode.

Compared to pristine MEH-PPV photodiodes, the addition of C_{60} lowers the average built in potential by 0.6 V, in accordance with the position of the C_{60}^- LUMO level relatively to the MEH-PPV polaron level. Therefore, an open circuit voltage as high as 0.72 V is not consistent with this picture. Variations of the ITO work function due to different production technologies as well as the unknown oxygen content in the different devices may contribute to these deviations in open circuit potential in different devices. It is well known that oxygen forms rectifying junctions in small organic molecule photovoltaic devices based on phtalocyanines.[35] The formation of space charge layers at the electrode/polymer interface[36] due to oxygen or other impuri-

ties may lead to local potentials influencing the open circuit potential. Systematic studies of the open circuit potential in these devices prove to be difficult and will not be addressed here.

By comparing the I_{sc} versus the PS concentration at various intensities [Fig. 5(a)] we see a sharp drop of the short circuit current for the cells with increasing PS concentration especially when both electroactive components are below their theoretical percolation threshold (80% PS).[37]

The dependence of the short circuit current on the incident light intensity [Fig. 5(b)] follows a power law $I_{sc} \sim I^{\alpha}$ with $\alpha \sim 0.5-0.7$. Scaling exponents α below 1 indicate either bimolecular recombination or saturation behavior. For the thin film photovoltaic devices investigated in this study both processes may be relevant. A detailed look [Fig. 5(c)] on selected devices reveals two different scaling regimes, one at low and one at high intensities. The PS free device scales linearly at low excitation intensities ($\alpha \sim 0.98$) while the exponent becomes lower ($\alpha \sim 0.55$) at intensities around ~ 10 mW/cm^2. The slightly higher scaling exponents in PS blended devices at high intensities may be explained by enhanced intermolecular spacing between the conjugated polymer and the fullerene due to dilution.

Figure 6 shows the total power conversion efficiency η_e of the cells under different illumination intensities. Calculation of η_e was performed using the relation

$$\eta_e = [V_{oc}(\mathrm{V}) * I_{sc}(\mathrm{A/cm^2}) * \mathrm{FF}] / [P_{in}(\mathrm{W/cm^2})], \tag{2}$$

where V_{oc}, I_{sc}, FF, P_{in} are the open circuit potential, short circuit current, filling factor, and incident light power, respectively. The filling factor was determined by calculation of the maximum power rectangular area under the $I-V$ curve in the fourth quadrant. The filling factor FF was calculated by Eq. (3):

$$\mathrm{FF} = V_p * I_p / (V_{oc} * I_{sc}) \tag{3}$$

with V_p and I_p as the intersection of the $I-V$ curve with the maximum power rectangle. Typical FF values for the investigated devices were between 0.3 and 0.35. With these data a total efficiency of 1.5% under 5 mW/cm^2 of 488 nm was calculated for the PS free device. At higher illumination intensities η_e decreases, but is still as high as 0.45% at 40 mW/cm^2. The PS free device shows a constant V_{oc} of 720 mV down to 5 mW/cm^2 irradiation intensity. The efficiency η_e of the cells decreased steadily with higher PS concentrations. A sharp drop occurred when one electroactive component was below the percolation threshold.

The spectrally resolved (IPCE) η_c,

$$\eta_c(\%) = 1240 * I_{sc}(\mu\mathrm{A/cm^2}) / \lambda(\mathrm{nm}) I(\mathrm{W/m^2}) \tag{4}$$

calculated from the spectrally resolved short circuit current values,[30] is plotted in Fig. 7 for the PS free device. In Eq. (4) I and λ denote the incident light intensity and the wavelength, respectively. The strong increase of the photocurrent at $h\nu \sim 2$ eV follows the absorption of the MDMO-PPV. From earlier studies on polymeric photovoltaic devices[38] it is known that two competing processes may determine the spectral response: the amount of absorbed light versus the location of the absorption region. As the film thickness

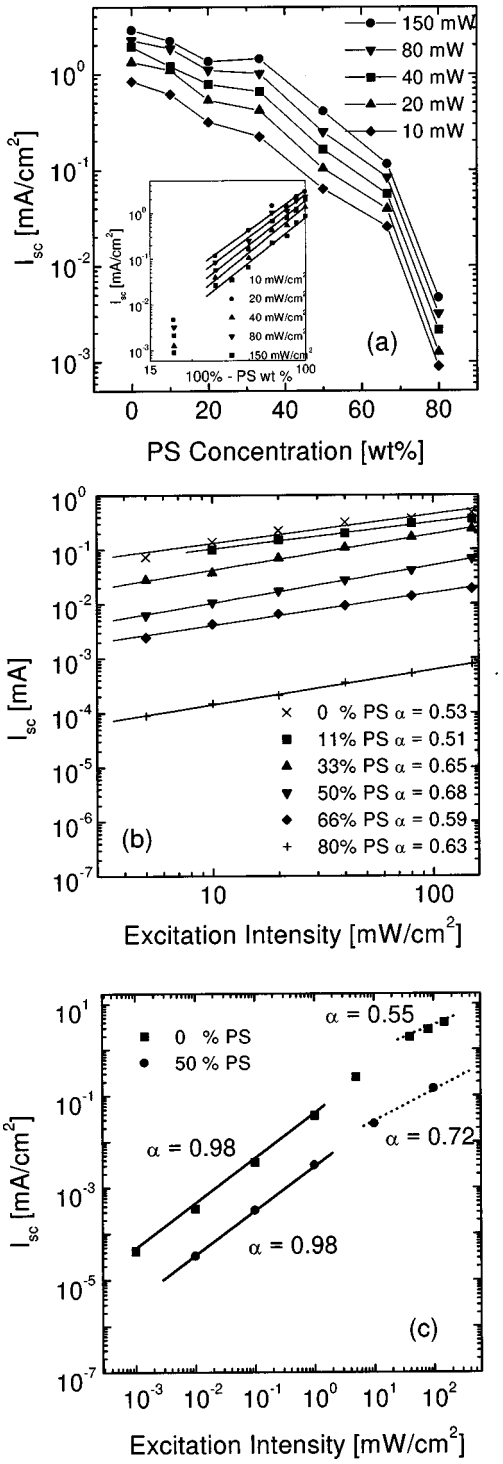

FIG. 5. (a) I_{sc} of various PS–MDMO-PPV–PCBM devices under different excitation intensity vs PS percentage. The inset shows the dependency of I_{sc} on the electroactive component concentrations (100%-PS wt %) in a log–log plot. Lines are power law fits according to $I_{sc} \sim (\mathrm{wt}\,\%)^{\alpha}$. Best fits are obtained with $\alpha \sim 3$. (b) I_{sc} of various PS–MDMO-PPV–PCBM devices vs excitation intensity at 488 nm. Lines are least square fits with a power law model $I_{sc} \sim I(488\,\mathrm{nm})^{\alpha}$. Concentrations of the samples as well as their scaling exponents are denoted. (c) I_{sc} of PS–MDMO-PPV–PCBM devices with 0% (■) and 50% (●) PS vs excitation intensity for 4 decades in intensity at 488 nm. Lines are least square fits for the separate scaling regions with a power law model $I_{sc} \sim I(488\,\mathrm{nm})^{\alpha}$. The exponents α are denoted.

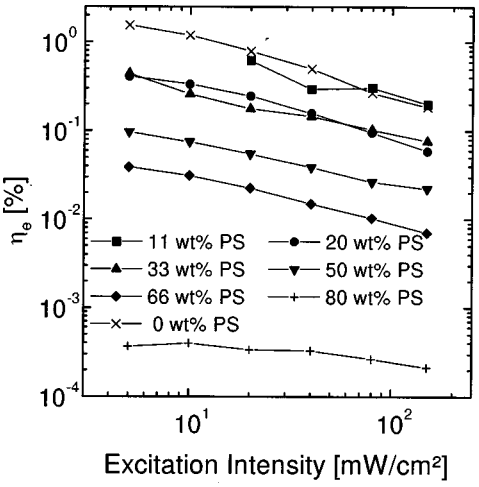

FIG. 6. Power efficiency η_e of various PS–MDMO-PPV–PCBM cells vs excitation intensity. Lines are drawn as a guide to the eye. Excitation is provided by Ar^+ laser at 488 nm.

grows, the photocurrent response is limited by absorption depth of the film, producing sharp maxima of the photocurrent at the onset of optical absorption and well pronounced minima of the photocurrent at the absorption maximum (filter effect). In Fig. 7 it is clearly seen that the investigated devices were not absorption depth limited in their photocurrent response. The inset of Fig. 7 shows the spectrally resolved photocurrent in the PS free device under forward and reverse bias. The complete symmetry of the spectral photocurrent with respect to the different signs of the applied voltage implies, that transport of the charges (photoconductivity for both signs) occurs with comparable efficiency for both networks. However, it is not possible to conclude which of the two networks may become the limiting one for thicker cells.

The PS free devices absorb typically less than 25% of the incident photons (measured in transmission geometry) at the MDMO-PPV maximum resulting in ~18% charge carriers per incident photon (IPCE). For three devices with 80%, 50%, and 0% PS content, the efficiency η_c as a function of the excitation wavelength is shown in Fig. 8(a). For the same devices, the dependence of η_c as well as η_e on the excitation intensity at a wavelength of 488 nm is shown in Fig. 8(b). At high excitation intensities the ratio of η_c/η_e is approximately 12. At lower excitation intensities this ratio increases due to the decrease of V_{oc}. The decrease of η_e and η_c with increasing PS concentration is consistent with the data shown in Fig. 5.

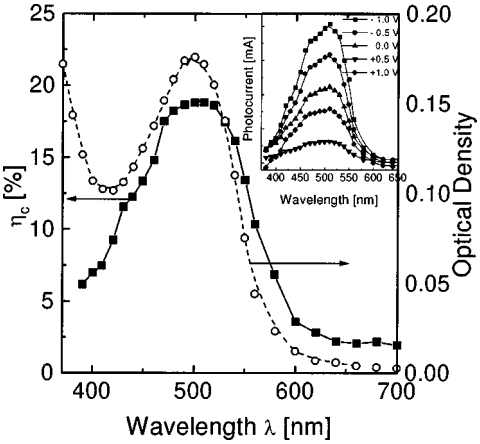

FIG. 7. Spectral resolved photon to carrier conversion efficiency η_c of a MDMO-PPV–PCBM (1:3) device. η_c was calculated according to Eq. (3). The inset shows the spectral resolved photocurrent under four different voltages (−1, −0.5, 0.5, and 1 V) and at short circuit conditions.

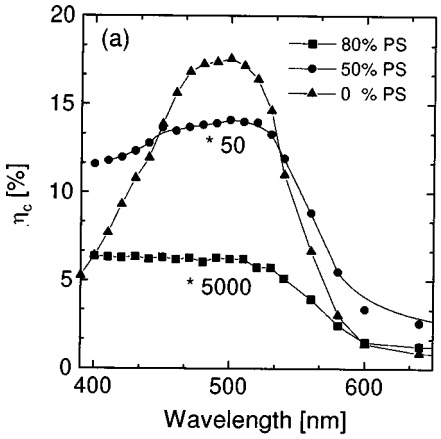

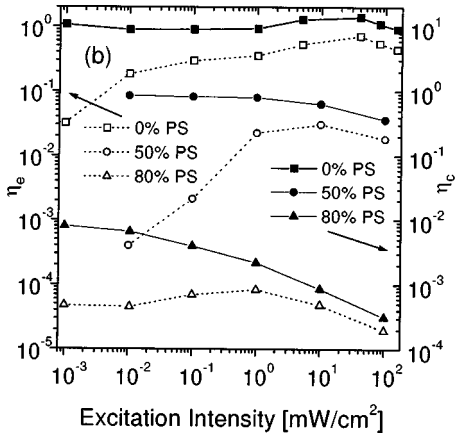

FIG. 8. (a) Carrier conversion efficiency η_c for three devices with 0%, 50%, and 80% PS. Data for the 50% and 80% device are multiplied by a factor 50 and 5000, respectively. (b) Excitation intensity dependence of η_e (left axis, open symbols) as well as η_c (right axis, full symbols) for devices with 0%, 50%, and 80% PS. Excitation is provided by defocused Ar^+ laser beam at 488 nm with neutral density filters.

IV. CONCLUSION

For large scale production of plastic solar cells, the rheological properties as well as the environmental stability will become relevant. For this purpose the behavior of highly efficient conjugated polymer/methanofullerene cells blended into a conventional polymer matrix were studied. Introducing small amounts of PS (10 wt%) did not change the efficiency of the cells significantly. Further increasing of the PS concentration resulted in a strong decrease of the I_{sc}. The percolation threshold for the interpenetrating network of the conjugated polymer/methanofullerene mixture in the host matrix determined the onset of a strongly enhanced photo-

voltaic response. The intensity dependence of the spectrally resolved photocurrent and of the short circuit current indicated that at higher light intensities enhanced annihilation of mobile charge carriers occurs. A proper choice of the host material may favorably tune the donor–acceptor network properties.

ACKNOWLEDGMENTS

This work was performed within the Christian Doppler Foundation's dedicated Laboratory for Plastic Solar Cells. Austrian Foundation for Advancement of Scientific Research (FWF Project No. P-12680-CHE) as well as The Netherlands Organization for Energy & Environment (NOVEM) are gratefully acknowledged for financial support.

[1] N. S. Sariciftci and A. J. Heeger, in *Handbook of Organic Conductive Molecules and Polymers*, edited by H. S. Nalwa (Wiley, New York, 1997), pp. 413–455.
[2] T. J. Kanicki, in *Handbook of Conducting Polymers*, edited by T. A. Skotheim (Dekker, New York, 1986), pp. 543–660.
[3] J. L. Bredas and R. Silbey, *Conjugated Polymers* (Kluwer Academic, Dodrecht, 1991).
[4] W. R. Salaneck, D. T. Clark, and E. J. Samuelsen, *Science and Application of Conducting Polymers* (Hilger, Bristol, 1991).
[5] N. S. Sariciftci, L. Smilowitz, A. J. Heeger, and F. Wudl, Science **258**, 1474 (1992); L. Smilowitz, N. S. Sariciftci, R. Wu, C. Gettinger, A. J. Heeger, and F. Wudl, Phys. Rev. B **47**, 13835 (1993).
[6] S. Morita, A. A. Zakhidov, and K. Yoshino, Solid State Commun. **82**, 249 (1992); K. Yoshino, X. H. Yin, S. Morita, T. Kawai, and A. A. Zakhidov, *ibid.* **85**, 85 (1993).
[7] B. Kraabel, J. C. Hummelen, D. Vacar, D. Moses, N. S. Sariciftci, A. J. Heeger, and F. Wudl, J. Chem. Phys. **104**, 4267 (1996).
[8] P. M. Allemand, A. Koch, F. Wudl, Y. Rubin, F. Diederich, M. M. Alvarez, S. J. Anz, and R. L. Whetten, J. Am. Chem. Soc. **113**, 1050 (1991).
[9] R. A. J. Janssen, J. C. Hummelen, K. Lee, K. Pakbaz, N. S. Sariciftci, A. J. Heeger, and F. Wudl, J. Chem. Phys. **103**, 788 (1995).
[10] C. W. Tang, Appl. Phys. Lett. **48**, 183 (1986).
[11] J. Rostalski and D. Meissner, in Proceedings of the 10th Workshop on Quantum Solar Energy Conversion QUANTSOL '98 (Bad Hofgastein, March 1998), edited by W. Kautek, J. Gobrecht, H. Kisch, S. Sariciftci, and C. Königstein.
[12] J. J. M. Halls, C. A. Walsh, N. C. Greenham, E. A. Marseglia, R. H. Friend, S. C. Moratti, and A. B. Holmes, Nature (London) **376**, 498 (1995).
[13] L. S. Roman, L. C. Chen, L. A. A. Pettersson, W. Mammo, M. R. Andersson, M. Johansson, and O. Inganäs, Synth. Met. (in press).
[14] G. Yu, J. Gao, J. C. Hummelen, F. Wudl, and A. J. Heeger, Science **270**, 1789 (1995).
[15] M. Granström, K. Petritsch, A. C. Aries, A. Lux, M. R. Andersson, and R. H. Friend, Nature (London) **395**, 257 (1998).
[16] J. Gao, F. Hide, and H. Wang, Synth. Met. **84**, 979 (1997).
[17] H. Böttger and V. V. Bryksin, *Hopping Conductions in Solids* (Akademie, Berlin, 1985).
[18] R. Zallen, *The Physics of Amorphous Solids* (Wiley, New York, 1983), Chap. 4.
[19] C. J. Brabec, F. Padinger, V. Dyakonov, J. C. Hummelen, R. A. J. Janssen, and N. S. Sariciftci, Proceedings of the International Winterschool on Electronic Properties of Novel Materials, Kirchberg, 1998, pp. 519–522.
[20] H. Neugebauer, C. J. Brabec, and N. S. Sariciftci, Synth. Met. (in press).
[21] C. H. Lee, G. Yu, D. Moses, K. Pakbaz, C. Zhang, N. S. Sariciftci, A. J. Heeger, and F. Wudl, Phys. Rev. B **48**, 15425 (1993).
[22] G. Yu, K. Pakbaz, and A. J. Heeger, Appl. Phys. Lett. **64**, 3422 (1994).
[23] J. C. Hummelen, B. W. Knight, F. Lepec, and F. Wudl, J. Org. Chem. **60**, 532 (1995).
[24] C. J. Brabec, D. Comoretto, I. Moggio, and G. Dellepiane, Chim. Ind. (Milan) **80**, 1301 (1998).
[25] E. Ehrenfreund, Z. Vardeny, O. Brafman, and B. Horovitz, Phys. Rev. B **36**, 1535 (1987).
[26] B. Tian, G. Zerbi, and K. Müllen, J. Chem. Phys. **95**, 3198 (1991).
[27] K. Lee, R. A. J. Janssen, N. S. Sariciftci, and A. J. Heeger, Phys. Rev. B **49**, 5781 (1994).
[28] Y. Wang and A. Suna, J. Phys. Chem. B **101**, 5627 (1997).
[29] I. D. Parker, J. Appl. Phys. **75**, 1656 (1993).
[30] L. S. Roman, M. R. Andersson, T. Yohannes, and O. Inganäs, Adv. Mater. **9**, 1164 (1997).
[31] K. Yoshino *et al.*, Synth. Met. **84**, 477 (1997).
[32] G. Yu and A. J. Heeger, J. Appl. Phys. **78**, 4510 (1995).
[33] G. Yu, C. Zhang, and A. J. Heeger, Appl. Phys. Lett. **64**, 1540 (1994).
[34] N. S. Sariciftci, D. Braun, C. Zhang, V. I. Srdanov, A. J. Heeger, G. Stucky, and F. Wudl, Appl. Phys. Lett. **62**, 585 (1993).
[35] J. Simon and J. J. Andre, *Molecular Semiconductors* (Springer, Berlin, 1985).
[36] W. R. Salaneck, S. Strafström, and J-L. Bredas, *Conjugated Polymer Surfaces and Interfaces* (Cambridge University Press, Cambridge, 1996).
[37] A. Aharony and D. Stauffer, *Introduction to Percolation Theory*, 2nd ed. (Taylor & Francis, London, 1993); A. J. Heeger, TRIP **3**, 39 (1995).
[38] R. N. Marks, J. J. M. Halls, D. D. C. Bradley, R. H. Friend, and A. B. Holmes, J. Phys.: Condens. Matter **6**, 1379 (1994).